

# Dark production of carbon monoxide (CO) from dissolved organic matter in the St. Lawrence estuarine system: Implication for the global coastal and blue water CO budgets

Yong Zhang,<sup>1,2</sup> Huixiang Xie,<sup>1</sup> Cédric G. Fichot,<sup>3</sup> and Guohua Chen<sup>4</sup>

Received 14 March 2008; revised 10 September 2008; accepted 9 October 2008; published 19 December 2008.

[1] We investigated the thermal (dark) production of carbon monoxide (CO) from dissolved organic matter (DOM) in the water column of the St. Lawrence estuarine system in spring 2007. The production rate,  $Q_{co}$ , decreased seaward horizontally and downward vertically.  $Q_{co}$  exhibited a positive, linear correlation with the abundance of chromophoric dissolved organic matter (CDOM). Terrestrial DOM was more efficient at producing CO than marine DOM. The temperature dependence of  $Q_{co}$  can be characterized by the Arrhenius equation with the activation energies of freshwater samples being higher than those of salty samples.  $Q_{co}$  remained relatively constant between pH 4–6, increased slowly between pH 6–8 and then rapidly with further rising pH. Ionic strength and iron chemistry had little influence on  $Q_{co}$ . An empirical equation, describing  $Q_{co}$  as a function of CDOM abundance, temperature, pH, and salinity, was established to evaluate CO dark production in the global coastal waters (depth < 200 m). The total coastal CO dark production from DOM was estimated to be from 0.46 to 1.50 Tg CO-C a<sup>-1</sup> (Tg carbon from CO a<sup>-1</sup>). We speculated the global oceanic (coastal plus open ocean) CO dark production to be in the range from 4.87 to 15.8 Tg CO-C a<sup>-1</sup> by extrapolating the coastal water-based results to blue waters (depth > 200 m). Both the coastal and global dark source strengths are significant compared to the corresponding photochemical CO source strengths (coastal: ~2.9 Tg CO-C a<sup>-1</sup>; global: ~50 Tg CO-C a<sup>-1</sup>). Steady state deepwater CO concentrations inferred from  $Q_{co}$  and microbial CO uptake rates are <0.1 nmol L<sup>-1</sup>.

**Citation:** Zhang, Y., H. Xie, C. G. Fichot, and G. Chen (2008), Dark production of carbon monoxide (CO) from dissolved organic matter in the St. Lawrence estuarine system: Implication for the global coastal and blue water CO budgets, *J. Geophys. Res.*, 113, C12020, doi:10.1029/2008JC004811.

## 1. Introduction

[2] The distribution and cycling of carbon monoxide (CO) in marine waters have been extensively investigated during the past several decades. Major findings are (1) photodegradation of chromophoric dissolved organic matter (CDOM) is the main source of CO in the upper ocean [Conrad *et al.*, 1982]; (2) microbial consumption is the major sink [Conrad *et al.*, 1982; Zafiriou *et al.*, 2003], while air-sea gas exchange is a minor loss term [Kettle, 1994; Bates *et al.*, 1995; Zafiriou *et al.*, 2008] and; (3) CO concentration ([CO]) in the surface ocean exhibits strong diel variations driven by diurnal fluctuations of the solar insolation and fast microbial removal

[Conrad *et al.*, 1982; Johnson and Bates, 1996; Zafiriou *et al.*, 2008]. Although the primary motivation of early studies of marine CO was to quantify its sea-to-air fluxes, recent interests in this species have been more focused on its impact on the marine dissolved organic carbon cycling [Mopper and Kieber, 2000; Zafiriou *et al.*, 2003; Stubbins *et al.*, 2006a; Xie *et al.*, 2008], its application as a proxy for estimating major but more difficult to measure CDOM photoproducts (e.g., CO<sub>2</sub> and biolabile organic carbon) [Miller and Zepp, 1995; Moran and Zepp, 1997], and its function in tuning coupled physical-optical-biological models [Kettle, 1994, 2000, 2005; Doney *et al.*, 1995].

[3] As the second most abundant inorganic carbon product of CDOM photochemistry, CO is reasonably constrained in terms of its photoproduction fluxes, particularly in open ocean waters [Bates *et al.*, 1995; Zafiriou *et al.*, 2003; Stubbins *et al.*, 2006a]. In contrast, thermal (dark) production of CO, another potentially important marine CO source, has drawn little attention. Xie *et al.* [2005] observed CO dark formation rates of  $0.21 \pm 0.21$  nmol L<sup>-1</sup> h<sup>-1</sup> in nine cyanide-poisoned Delaware Bay water samples. Significant CO dark production was also inferred from modeling upper ocean CO cycles [Kettle, 1994, 2005]. The dark production term is

<sup>1</sup>Institut des Sciences de la Mer de Rimouski, Université du Québec à Rimouski, Rimouski, Québec, Canada.

<sup>2</sup>Yantai Institute of Coastal Zone Research for Sustainable Development, Chinese Academy of Sciences, Yantai, China.

<sup>3</sup>Department of Marine Sciences, University of Georgia, Athens, Georgia, USA.

<sup>4</sup>College of Chemistry and Chemical Engineering, Ocean University of China, Qingdao, China.

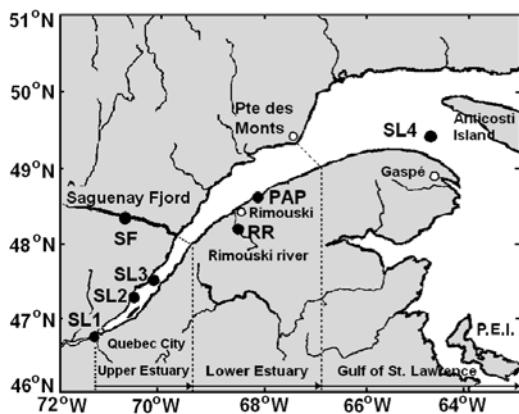


**Figure 1.** Sampling locations in the St. Lawrence estuarine system.

often critical to rationalize model-data discrepancies and greatly affects the values of CO photoproduction and microbial uptake rates derived from inverse modeling approaches [Kettle, 2005]. Therefore, the lack of quantitative knowledge of this pathway seriously limits modeling and may add substantial uncertainties to the global marine CO budget.

[4] Here we report the spatial variation of the abiotic, dark production of CO in the St. Lawrence estuarine system, evaluate the principal factors affecting this process, and discuss the implication of CO dark production for the oceanic CO cycle and budget. To our knowledge, this is the first relatively systematic study of CO dark production in natural waters.

## 2. Methods

### 2.1. Study Area

[5] The estuary and Gulf of St. Lawrence, referred to as the St. Lawrence estuarine system (SLES) herein, is a semiclosed water body with connections to the Atlantic Ocean in the east (Figure 1). With an area of 10,800 km<sup>2</sup> and a drainage basin of ~1.3 million km<sup>2</sup>, the St. Lawrence is the second largest river system in North America. Over a relatively small horizontal scale (~1200 km), surface water in the SLES transitions from freshwater-dominated CASE 2 water in the estuary to oceanic water-dominated CASE 1 water in the Gulf [Nieke et al., 1997]. The water column is fairly well mixed in the upper estuary (Quebec City to the mouth of the Saguenay Fjord) but highly stratified, except in winter, in the lower estuary (the mouth of Saguenay Fjord to Pointe-des-Monts), the Gulf, and the Saguenay Fjord. The Saguenay Fjord is the principal tributary of the SLES with the fjord's surface water being highly enriched with CDOM. Dissolved organic matter (DOM) in the surface waters of the St. Lawrence estuary and Saguenay Fjord has been shown to be mainly terrigenous while marine contribution to the DOM pool is important below the thermocline [Tremblay, 2003]. Conservative behavior of CDOM and dissolved organic carbon (DOC) during estuarine mixing in the SLES has been observed [Nieke et al., 1997; Zhang et al., 2006]. Limited data also indicates that CDOM linearly correlates with DOC in this area [Zhang et al., 2006].

### 2.2. Sampling

[6] Sampling was conducted aboard the research ship *Coriolis II* between 3 and 9 May 2007. Four stations (SL1–SL4) were distributed along an axial transect from the upstream limit of the estuary near Quebec City to the Gulf (Figure 1). The same cruise also visited a site in the Saguenay Fjord (station SF in Figure 1). Water samples were taken using 12-L Niskin bottles attached to a CTD rosette. They were gravity-filtered using sterile Pall AcroPak 500 capsules sequentially containing 0.8- $\mu$ m and 0.2- $\mu$ m polyethersulfone membrane filters. The capsules were connected to the Niskin bottles' spigot with clean silicon tubing. Prior to sample collection, the capsules were thoroughly rinsed with Nanopure water to avoid potential contamination. The filtered samples were transferred into acid-cleaned 4-L clear glass bottles or 20-L collapsible polyethylene bags (Cole-Parmer) that were protected against sunlight. Samples in the glass bottles were used immediately upon collection for shipboard incubations. Because of the short duration of the cruise and technical constraints, those samples in the plastic bags had to be stored in darkness at 4°C and brought back to the laboratory at Rimouski for land-based incubations. Sampling depths for each station visited, along with other related parameters, are shown in Table 1.

### 2.3. Shipboard Incubations

[7] BOD bottles (300 mL) were used as incubating vessels for both shipboard and land-based incubation experiments. Prior to sample incubations, the bottles were soaked in 10% HCl for over 24 h and rinsed thoroughly with Nanopure water. Incubations consisting of filtered Nanopure water resulted in negligible CO production. Shipboard incubations were conducted to measure CO dark production rates,  $Q_{CO}$ , at in situ temperatures and pH at stations SL1, SL3, SL4 and SF. Each sample was purged in the dark with CO-free air (medical grade) to minimize background [CO] and then siphoned through a 1/4" Teflon tube into seven BOD bottles under dimmed room light. The bottles were first rinsed with the sample water and then overflowed with the sample by ~2 times their volumes before they were closed without headspace. During the sample transfer, the Teflon tube was inserted down to near the bottom of the bottles and bubbles were avoided. [CO] in one bottle was measured immediately after the sample transfer and was subtracted as background [CO] (<0.2 nmol L<sup>-1</sup>). The remaining six bottles were incubated at constant temperatures ( $\pm 0.5^\circ$ C) by immersing them in a circulating water bath modified from a Coleman cooler. The water bath was completely darkened with opaque foam and black garbage bags. Samples were sacrificed sequentially for [CO] measurement, usually three time points, each with duplicate.

### 2.4. Land-Based Laboratory Incubations

[8] Samples brought back from the *Coriolis II* cruise were refiltered with 0.2- $\mu$ m polyethersulfone membrane filters immediately before they were incubated. The purposes of these incubations were to determine the effects of CDOM abundance ([CDOM]), temperature ( $T$ ) and pH on  $Q_{CO}$ . They were performed on water samples from stations SL1–SL4 and SF and followed exactly the same procedure

**Table 1.** Stations, Sampling Depth, Water Temperature ( $T$ ), Salinity, pH,  $a_{350}$ , Dark Production Rate ( $Q_{co}$ ), and Sample Storage Time

Station	Depth (m)	$T$ (°C)	Salinity	pH	$a_{350}$ <sup>a</sup> ( $m^{-1}$ )	$Q_{co}$ <sup>b</sup> ( $nmol L^{-1} h^{-1}$ )	Storage Time (days)
<i>Shipboard Incubation</i>							
SL1	2	9.49	0.1	7.76	6.80	0.11	0
SL3	2	3.70	18.5	7.81	3.36	0.015	0
SL3	50	0.91	29.1	7.79	1.31	0.0021	0
SL4	2	1.94	31.6	8.10	0.56	u.d.	0
SL4	20	0.30	31.9	8.00	0.56	u.d.	0
SL4	300	5.42	34.7	7.75	0.23	u.d.	0
SF	2	5.54	4.7	7.59	15.32	0.12	0
SF	10	2.00	20.6	7.55	8.03	0.060	0
SF	150	1.68	31.1	7.62	1.42	0.0015	0
<i>[CDOM] Series Incubation</i>							
SL1	2	20.0	0.1	7.86	6.80	0.26	11
SL2	2	20.0	12.9	7.86	4.21	0.15	9
SL3	2	20.0	18.5	7.86	3.36	0.10	9
SL4	2	20.0	31.6	7.86	0.56	0.0059	11
SF	2	20.0	4.7	7.86	15.32	0.55	9
PAP	0	20.0	25.6	7.86	2.42	0.062	15
<i>T Series Incubation</i>							
SL1	2	2.0	0.1	7.76	6.80	0.016	15
SL1	2	10.0	0.1	7.76	6.80	0.067	15
SL1	2	20.0	0.1	7.76	6.80	0.21	16
SL1	2	30.0	0.1	7.76	6.80	0.99	16
SL4	300	2.0	34.7	7.75	0.23	u.d.	18
SL4	300	10.0	34.7	7.75	0.23	0.0009	18
SL4	300	20.0	34.7	7.75	0.23	0.0042	19
SL4	300	30.0	34.7	7.75	0.23	0.0073	19
SF	2	2.0	4.7	7.59	15.32	0.022	16
SF	2	10.0	4.7	7.59	15.32	0.097	16
SF	2	20.0	4.7	7.59	15.32	0.53	17
SF	2	30.0	4.7	7.59	15.32	2.08	17
PAP	0	2.0	25.6	7.97	2.42	0.0038	19
PAP	0	10.0	25.6	7.97	2.42	0.016	19
PAP	0	20.0	25.6	7.97	2.42	0.067	20
PAP	0	30.0	25.6	7.97	2.42	0.19	20
<i>pH Series Incubation</i>							
SL1	2	20.0	0.1	4.00	6.80	0.18	24
SL1	2	20.0	0.1	6.00	6.80	0.19	24
SL1	2	20.0	0.1	8.00	6.80	0.27	24
SL1	2	20.0	0.1	9.00	6.80	0.62	25
SL1	2	20.0	0.1	10.00	6.80	1.81	25
SL4	300	20.0	34.7	4.00	0.23	0.0031	25
SL4	300	20.0	34.7	6.00	0.23	0.0024	25
SL4	300	20.0	34.7	8.00	0.23	0.0033	25
SL4	300	20.0	34.7	9.00	0.23	0.0042	26
SL4	300	20.0	34.7	10.00	0.23	0.0072	26
SF	2	20.0	4.7	4.00	15.32	0.27	26
SF	2	20.0	4.7	6.00	15.32	0.19	26
SF	2	20.0	4.7	8.00	15.32	0.58	26
SF	2	20.0	4.7	8.50	15.32	1.03	26
SF	2	20.0	4.7	9.00	15.32	1.76	26
SF	2	20.0	4.7	10.00	15.32	4.55	26
PAP	0	20.0	25.6	4.00	2.42	0.066	15
PAP	0	20.0	25.6	6.00	2.42	0.038	15
PAP	0	20.0	25.6	8.00	2.42	0.08	15
PAP	0	20.0	25.6	8.50	2.42	0.15	15
PAP	0	20.0	25.6	9.00	2.42	0.26	15
PAP	0	20.0	25.6	10.00	2.42	0.53	15

<sup>a</sup>Here  $a_{350}$  for the pH series was not monitored after pH adjustment. After-study tests indicated that the effect of pH adjustment on  $a_{350}$  is within  $\pm 12\%$  of the original values. Lowering pH decreased  $a_{350}$ , while raising pH increased it.

<sup>b</sup>Note that u.d. indicates undetectable.

as for the shipboard incubations. The [CDOM] series study was realized by incubating samples from various stations at constant  $T$  (20.0°C) and pH (7.86), the median of the samples' original pH values. The  $T$  series incubations were conducted at constant pH (sample's original pH) but at varying  $T$ : 2.0, 10.0, 20.0 and 30°C. The pH series incubations were performed at constant  $T$  (20.0°C) but at pH varying from 4.0 to 10.0 (Table 1). HCl (1 N or 5 N) or NaOH (1 N or 5 N) was used to adjust pH, if required.

[9] The land-based incubations were carried out within 9–26 days (average: 19 days) of sample collection, with each set of incubation being completed usually within 1–3 days (Table 1). An assessment of the effect of sample storage on  $Q_{co}$  was conducted on a surface water sample taken from Pointe-au-Père, Rimouski, situated on the south shore of the St. Lawrence River (station PAP in Figure 1).  $Q_{co}$  (20°C) in this sample was determined, using the same procedure as described above, at storage time of 1, 3, 5, 12 and 22 days. Note that [CDOM],  $T$  and pH series incubations were also performed on the PAP water (Table 1).

[10] The effects of ionic strength ( $I$ ) and iron on CO dark production were investigated using water freshly collected from the highly colored Rimouski River (station RR in Figure 1) containing a moderate level of iron (total iron:  $3.3 \mu mol L^{-1}$ ) [Lou, 2005]. To test the role of ionic strength, aliquots of the filtered (0.2  $\mu m$ ) RR water were added with varying amounts of NaCl (reagent grade, BDH) to form an  $I$  series of 0.0, 0.2, 0.4, 0.6 and 1.0  $mol L^{-1}$  and then incubated at 20°C. The influence of iron chemistry was assessed by amending the water with 100  $\mu mol L^{-1}$  deferoxamine mesylate (DFOM) (reagent grade, Sigma-Aldrich), a strong Fe (III) -complexing ligand [Gao and Zepp, 1998; Xie *et al.*, 2004]. The water was left in the dark for 24 h to allow the completion of the complexing process before it was incubated (20°C) along with a DFOM-free control. Incubation of Nanopure water spiked with 100  $\mu mol L^{-1}$  DFOM did not produce significant CO.

## 2.5. Analysis

[11] Incubating BOD bottles to be analyzed for CO were brought rapidly to laboratory temperatures in a completely opaque water bath. A subsample was drawn from the bottom of each BOD bottle into a 50-mL glass syringe (Perfectum) via a short length of 1/8" OD Teflon tubing. The syringe was flushed twice with the sample water before being filled, the last flush being free from air bubbles. The sample was analyzed using a headspace method (1: 6 gas: water ratio) for CO extraction and a modified Trace Analytical TA3000 reduction gas analyzer for CO quantification [Xie *et al.*, 2002]. The syringe was protected against light during sampling and analysis. CDOM absorbance spectra were recorded at room temperature from 200 to 800 nm at 1 nm increments using a Perkin-Elmer lambda-35 dual beam UV-visible spectrometer fitted with 10 cm quartz cells and referenced to Nanopure water. A baseline correction was applied by subtracting the absorbance value averaged over an interval of 5 nm around 685 nm from all the spectral values [Babin *et al.*, 2003]. Absorption coefficients,  $a_{\lambda}$  ( $m^{-1}$ ) ( $\lambda$ : wavelength in nanometers), were calculated as 2.303 times the absorbance divided by the cell's light path length in meters. The lower detection limit of the absorption coefficient measurement was 0.03  $m^{-1}$ .

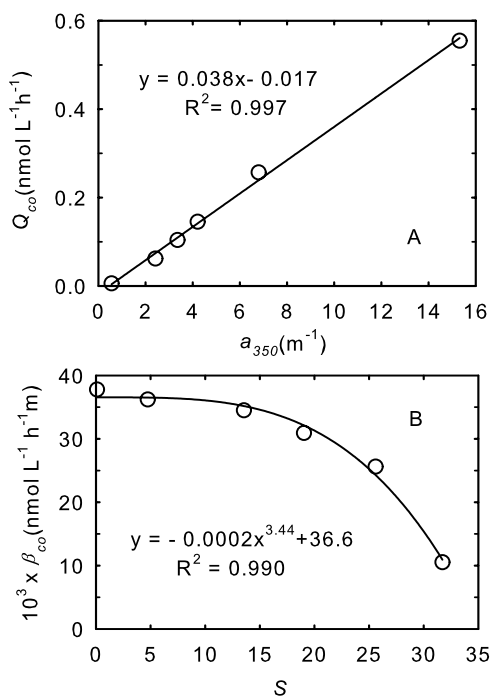


**Figure 2.** (a) Dark production rate,  $Q_{co}$ , as a function of CDOM absorption coefficient at 350 nm,  $a_{350}$ . (b) The CDOM-normalized CO dark production,  $\beta_{co}$  (i.e.,  $Q_{co} \div a_{350}$ ), as a function of salinity,  $S$ .  $Q_{co}$  was determined at pH = 7.86 and  $T = 20^\circ\text{C}$ .

Salinity was determined with a Portasal (model 8410A) salinometer. A ThermOrion pH meter (model 420) fitted with a Ross Orion combination electrode was used to determine pH; the system was standardized with three NIST buffers at pH 4.01, 7.00, and 10.01.

### 3. Results and Discussion

[12] In incubations where significant CO dark production was detected (53 out of 57 incubations total), [CO] always increased linearly with time over the incubation durations. The  $Q_{co}$  values derived from least squares regression analysis between [CO] and incubation time are included in Table 1. Plots of [CO] versus incubation time and parameters for the best fit equations are given in Auxiliary Material.<sup>1</sup>

#### 3.1. Spatial Distribution of $Q_{co}$

[13] Samples for shipboard incubations spanned a relatively small pH range (7.55–8.10), intermediate  $T$  bounds (0.30–9.49°C), and large variations of salinity (0.1–34.7) and [CDOM] ( $a_{350}$ : 0.23–15.32 m<sup>-1</sup>) (Table 1). They covered various water masses represented by highly colored riverine water at station SF (2 m), relatively low [CDOM] freshwater at SL1, estuarine water at SL3 (2 m) and PAP, coastal water at SL4 (2 m), and largely oceanic water at the bottom of SL4 (300 m) (Figure 1). As these samples were incubated in situ  $T$  and pH, their  $Q_{co}$  values are considered to approximate in situ rates. In the surface mixed layer,

$Q_{co}$  (2 m deep) was the highest (0.12 nmol L<sup>-1</sup> h<sup>-1</sup>) in the Saguenay Fjord (station SF), decreased progressively from the upstream limit of the SLES (station SL1: 0.11 nmol L<sup>-1</sup> h<sup>-1</sup>) to the Gulf (station SL4: undetectable) (Table 1), in accordance with the descending [CDOM] and  $T$  toward the sea. Vertically,  $Q_{co}$  dropped by  $\sim 7$  times from 2 to 50 m at SL3, and by 2 times from 2 to 10 m and  $\sim 92$  times from 2 to 150 m at SF. The decrease in  $Q_{co}$  with depth was in line with the vertical distributions of [CDOM] and  $T$  (Table 1). These  $Q_{co}$  profiles are similar to those of carbonyl sulfide (COS) dark production in the Northeast Atlantic, which is approximately 1 order of magnitude weaker in deep waters than in the mixed layer [Flock and Andreae, 1996]. CO dark production was undetectable at all three depths sampled at station SL4 due apparently to the combination of low CO precursor concentrations (as reflected by low [CDOM]) and low water  $T$  (Table 1).

### 3.2. Factors Affecting CO Dark Production

#### 3.2.1. $Q_{co}$ Versus [CDOM]

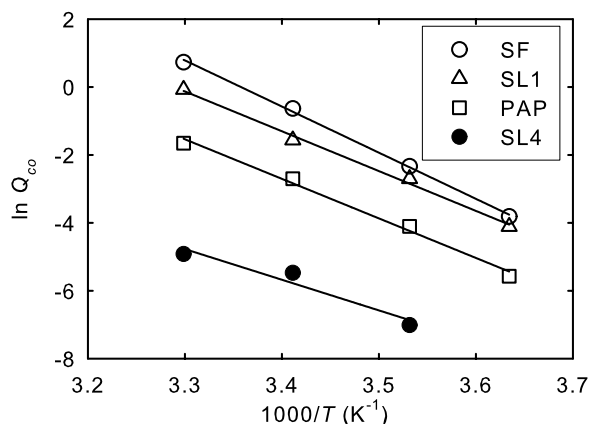
[14] For samples whose  $Q_{co}$  was determined at fixed  $T$  and pH ([CDOM] series in Table 1),  $Q_{co}$  should be dictated by the abundance and reactivity of CO precursors, ionic strength, and other chemical variables (e.g., certain metal ions) that could influence the thermal reactions responsible for generating CO. Statistical analysis indicates that  $a_{350}$  accounts for 99.7% of the  $Q_{co}$  variability (Figure 2). This suggests that organic substrates were a prevailing factor in controlling CO dark production and that [CDOM] is a good proxy for the abundance of CO precursors, as is the case of [CDOM] serving a good indicator of organic substrates for COS dark production in the Sargasso Sea [Von Hobe et al., 2001]. This leaves ionic strength and other chemical variables to be minor factors, as confirmed by separate tests (see below). The [CDOM]-normalized  $Q_{co}$ ,  $\beta_{co}$ , decreased with salinity (Figure 2), an observation similar to that for the photoreactivity of CDOM with respect to CO photoproduction [Zhang et al., 2006]. This trend points to CO precursors of marine origin being less efficient than their terrestrial counterparts, yet the convex upward shape of the  $\beta_{co}$  versus salinity ( $S$ ) curve implies that, besides dilution, other factors impacted  $\beta_{co}$ . Such factors include changes in the composition and diagenetic state of terrestrial DOM during estuarine transport due to photochemical and biological processes, flocculation, and mixing with DOM of different origins, such as marine DOM [Hernes and Benner, 2003].

[15] In principle DOC could be a better proxy than CDOM for CO precursors since CDOM is only a portion (though usually a large portion in estuarine and coastal waters) of the whole DOM pool. Unfortunately, instrumental problems result in no reliable DOC data from this study. The excellent correlation between  $Q_{co}$  and  $a_{350}$ , however, suggests that CO precursors were mainly present in CDOM or that [CDOM] linearly correlated with the DOC concentration ([DOC]). Data collected by Zhang et al. [2006] in summer 2004 did show a linear correlation between  $a_{350}$  and [DOC] (mg L<sup>-1</sup>) in the same study area ( $a_{350} = 0.63 \times [\text{DOC}] + 0.51$ ,  $R^2 = 0.986$ ,  $n = 13$ ).

#### 3.2.2. Temperature Dependence

[16] The  $T$  effect on CO dark production was assessed on four water samples from stations SL1 (2 m), SF (2 m), PAP (0 m) and SL4 (300 m) representing four differing water

<sup>1</sup>Auxiliary materials are available in the HTML. doi:10.1029/2008JC004811.



$$\text{SF: } y = -13.6x + 43.7, R^2 = 0.998$$

$$\text{SL1: } y = -11.7x + 38.6, R^2 = 0.995$$

$$\text{PAP: } y = -11.6x + 36.9, R^2 = 0.992$$

$$\text{SL4: } y = -9.03x + 25.0, R^2 = 0.941$$

**Figure 3.** Arrhenius plots of CO dark production rates.  $Q_{co}$  was determined at sample's original pH and salinity. Lines are the best fits of the data.

masses (see section 3.1.). Significant CO dark production was found in all incubations except for the SL4 sample incubated at 2.0°C ( $T$  series in Table 1) due obviously to the low temperature. As expected, the  $Q_{co}$ - $T$  relationship follows the linear Arrhenius behavior (Figure 3). The activation energy,  $E_a$ , in ascending order, is station SL4 (75.1 kJ mol<sup>-1</sup>), PAP (96.4 kJ mol<sup>-1</sup>), SL1 (97.5 kJ mol<sup>-1</sup>), and SF (113.0 kJ mol<sup>-1</sup>).  $E_a$  for freshwater samples is therefore considerably higher than for the most saline water (SL4), a trend similar to  $E_a$  for CO photoproduction [Zhang *et al.*, 2006]. However,  $E_a$  for dark production is much higher than that for photoproduction (<20 kJ mol<sup>-1</sup>) [Zhang *et al.*, 2006]. For a 20°C increase in  $T$ , CO dark production should increase by ~22 times at station SF, ~16 times at SL1, and ~8 times at SL4. In contrast, a similar elevation of  $T$  would raise CO photoproduction merely by <70% [Zhang *et al.*, 2006].

[17] In the SLES, the summer-winter surface  $T$  difference is ~22°C at the upstream limit (Quebec City) and ~18°C in the Gulf, causing  $Q_{co}$  to be 22 times and 6 times higher, respectively, in summer than in winter. Similar seasonal  $T$ -driving variations in CO dark production are expected for midlatitude and high-latitude inland, estuarine, and near-shore aquatic systems. However, the effect of  $T$  seasonality in the open ocean, maximal in midlatitudes (~6°C), should be relatively small (~2 times) if our  $Q_{co}$ - $T$  relationship for station SL4 is applied.

### 3.2.3. Effect of pH

[18] The same samples examined for the  $T$  effect were used to assess the pH effect. The shapes of all four  $Q_{co}$  versus pH curves are alike (Figure 4). From pH 4.0 to 6.0  $Q_{co}$  slightly decreased at stations SL4, PAP, and SF but remained stable at SL1. The production rate went up slowly from pH 6.0 to 8.0 and then rapidly with further increasing pH. The  $Q_{co}$ -pH relationships can be well described by a three-parameter exponential (Figure 4). Mopper *et al.* [2006] observed a similar pH dependence of CO photopro-

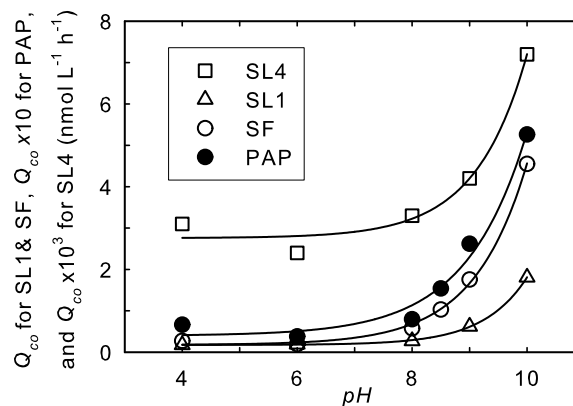
duction in a CDOM-rich swamp sample, showing minimum photoproduction in pH 4.5–6 and maximum at pH ~8 (no > 8 values were tested). They ascribed this pH dependence to structural changes in humic macromolecules, e.g., micelle formation at pH 4.5–6, a mechanism that might also be responsible for low CO dark production at low pH. In addition, protonation of potential CO-producing functionalities on DOM (e.g., ketone and aldehyde groups) at low pH could also reduce CO dark production by preventing them from undergoing this process.

### 3.2.4. Effects of Sample Storage, Ionic Strength, and Iron

[19]  $Q_{co}$  in the PAP water decreased nonlinearly with storage time according to  $Q_{co} = 0.051 + 0.044 \cdot \exp(-0.10 t)$  ( $R^2 = 0.996$ ,  $n = 5$ ), where  $t$  is storage time in days. The decrease was fast initially and leveled off afterward, suggesting the rapid loss of the most reactive CO precursors during the initial storage. If this equation also applies to other samples,  $Q_{co}$  from land-based incubations would be underestimated by 24–40% (average: 36%).

[20] At ionic strengths ( $I$ ) of 0, 0.2, 0.4, 0.6 and 1.0 mol L<sup>-1</sup>,  $Q_{co}$  (mean ± SD,  $n = 4$ ) in the RR sample was  $0.43 \pm 0.01$ ,  $0.39 \pm 0.01$ ,  $0.42 \pm 0.04$ ,  $0.40 \pm 0.01$ , and  $0.41 \pm 0.04$  nmol L<sup>-1</sup> h<sup>-1</sup>, respectively. Ionic strength therefore did not significantly affect CO dark production, contrary to the inverse relationship between  $I$  and CO photoproduction observed by Minor *et al.* [2006]. Conformational change of DOM and/or alteration in iron photochemistry, which are postulated to cause the effect of ionic strength on CO photoproduction [Minor *et al.*, 2006], did not seem to influence the CO dark production.

[21]  $Q_{co}$  in the DFOM-added RR sample was only slightly (9%) lower than in the original sample, indicative of minor influence of iron on the CO dark production process. Again, this contrasts the strong enhancement of CO photoproduc-



The best fit equation:  $y = a + b \cdot \exp(c \cdot x)$

station	y	a	b	c	R <sup>2</sup>
SL4	$Q_{co} \times 10^3$	2.76	$5.72 \times 10^{-5}$	1.13	0.980
SF	$Q_{co}$	0.177	$8.93 \times 10^{-5}$	1.08	0.998
SL1	$Q_{co}$	0.175	$3.13 \times 10^{-6}$	1.32	1.00
PAP	$Q_{co} \times 10$	0.398	$4.00 \times 10^{-4}$	0.95	0.982

**Figure 4.** Plots of  $Q_{co}$  versus pH.  $Q_{co}$  was determined at 20°C. Lines are the best fits of the data.

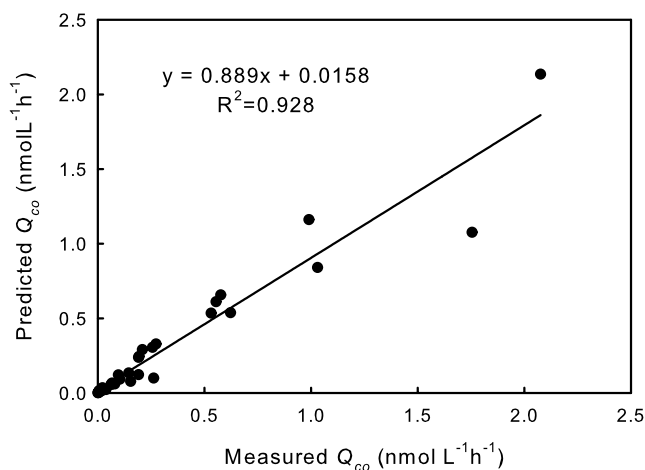


**Figure 5.**  $Q_{co}$  values predicted from equation (1) in the text versus measured values. Line is the best fit of the data.

tion by iron observed in the Rimouski River [Lou, 2005] and in some organic-rich rivers in the southeastern United States [Gao and Zepp, 1998; Xie et al., 2004].

### 3.3. Implication for the Global Coastal Water CO Budget

[22] Taking into account the  $S$ ,  $T$ , and pH dependences, we derived the following equation for predicting the CDOM-normalized CO dark production rate,  $\beta_{co}$ :

$$\ln(\beta_{co} \times 10^3) = -12305 T^{-1} + 0.494 \text{ pH} - 0.0257 S + 41.9 \quad (1)$$

where  $\beta_{co}$  is in  $\text{nmol m L}^{-1} \text{ h}^{-1}$ , and  $T$  in Kelvin. The pH data used for fitting equation (1) are in the range 6.0–9.0. If  $a_{350}$  is known,  $Q_{co}$  can be calculated as  $\beta_{co} \times a_{350}$ . Statistically,  $T$ ,  $S$  and pH can explain 92.8% of the  $Q_{co}$  variance (Figure 5). The unaccounted variance could largely originate from varying sample storage times (Table 1). The validity of equation (1) was checked by predicting the  $Q_{co}$  values for the SLES stations where in situ rates had been measured (Table 1). Compared to the in situ rates, the predicted rates are 31–49% lower at stations SL1, SL3 (both 2 and 50 m) and SF (2 m), 80% lower at station SF (10 m), and 10% higher at station SF (150 m). Therefore, the majority (4 out of 6) of the predicted values are  $\sim 40\%$  lower, which is close to the 36% decrease in  $Q_{co}$  inferred from the sample storage test (section 3.2.4).

[23] As equation (1) was based on samples with salinity ( $\leq 34.7$ ) and  $a_{350}$  ( $\geq 0.23 \text{ m}^{-1}$ ) ranges being typical of coastal waters, we assume that equation (1) is applicable to coastal oceans other than the SLES. To estimate the global coastal CO dark production flux, coastal oceans (depth < 200 m) are divided into various latitudinal zones and two depth layers: the surface mixed layer (ML) ( $27.5^\circ\text{S}$ – $27.5^\circ\text{N}$ : 0–50 m;  $> 27.5^\circ\text{N}$  (S): 0–100 m) and the subsurface layer (Table 2). Area-weighted annual mean  $T$  and zonal areas were derived from Levitus [1982], pH is set at 7.8, and salinity at 28.0. A modified version of the SeaUV algorithm [Fichot et al., 2008] was implemented on a 10-year

(September 1997 to August 2007) data set of SeaWiFS ocean color (monthly binned at  $9 \times 9 \text{ km}$ ) to derive  $1^\circ \times 1^\circ$  monthly climatologies of surface-ocean  $a_{350}$ . The published SeaUV algorithm was used to estimate the diffuse attenuation coefficient at 320 nm,  $Kd_{320}$ , from which  $a_{350}$  was computed by using a constant ratio  $a_{320} \div Kd_{320} = 0.68$  and a CDOM spectral slope coefficient of  $-0.0194 \text{ nm}^{-1}$ . The values for the ratio and spectral slope coefficient were derived from the data set used in the development of the SeaUV algorithm. The monthly climatologies were used to compute an annual average for each of the latitudinal zones shown in Table 2. The uncertainty in the remotely sensed  $a_{350}$  values was estimated to be  $\pm 32\%$  [Fichot, 2004]. [CDOM] was assumed to be vertically homogeneous.

[24] Equation (1) was then used to calculate  $Q_{co}$  for each zone and layer (with 50-m depth resolution). Equation (1) yields significant CO dark production in all zones and layers compared to the  $Q_{co}$  value of  $8.0 \times 10^{-4} \text{ nmol L}^{-1} \text{ h}^{-1}$ , which is the upper limit predicted for the SLES samples with undetectable CO dark production (Table 1). The per-unit-volume rates are converted to the annual depth- and area-integrated CO dark production fluxes (Table 2). The total flux is estimated as  $0.68 \text{ Tg CO-C a}^{-1}$ , of which  $0.54 \text{ Tg CO-C a}^{-1}$  is produced in the ML and  $0.14 \text{ Tg CO-C a}^{-1}$  below it. Latitudinally, CO dark production decreases poleward:  $0.34 \text{ Tg CO-C a}^{-1}$  in the tropics,  $0.19 \text{ Tg CO-C a}^{-1}$  in the subtropics,  $0.10 \text{ Tg CO-C a}^{-1}$  in the temperate zones, and  $0.051 \text{ Tg CO-C a}^{-1}$  in the high-latitude areas. This pattern suggests that temperature outweighs CDOM in controlling the CO dark production since the latitudinal distributions of  $a_{350}$  and  $T$  show roughly opposite trends (Table 2) and pH and  $S$  are set to be constant. Note that all these estimates do not account for the sample storage effect as shown above and hence are likely lower limits. If the storage-linked underestimation for the PAP sample ( $\sim 40\%$ ) also applies to other coastal waters, these values should be raised by 67%, giving a total coastal dark source of  $1.14 \text{ Tg CO-C a}^{-1}$ . Considering the storage effect-corrected value as the upper limit, we estimated the global coastal CO dark production from DOM to be in the range  $0.68$ – $1.14 \text{ Tg CO-}$

**Table 2.** Annual CO Dark Production in Global Coastal Waters<sup>a</sup>

Region	Layer (m)	Area ( $10^4 \text{ km}^2$ )	$T$ ( $^\circ\text{C}$ )	$a_{350}$ ( $\text{m}^{-1}$ )	CO ( $\text{Tg C a}^{-1}$ )
42.5–57.5°N	0–100	212.4	6.6	0.57	0.04
	100–200	39.3	5.4	0.57	0.006
27.5–42.5°N	0–100	108.4	16.0	0.46	0.06
	100–200	24.0	11.6	0.46	0.007
12.5–27.5°N	0–50	153.6	24.5	0.33	0.11
	50–200	43.8	19.9	0.33	0.05
0–12.5°N	0–50	198.0	27.0	0.29	0.17
	50–200	44.4	18.7	0.29	0.04
12.5–0°S	0–50	168.6	26.4	0.25	0.11
	50–200	26.8	20.0	0.25	0.02
27.5–12.5°S	0–50	61.2	23.2	0.23	0.02
	50–200	16.4	19.7	0.23	0.012
42.5–27.5°S	0–100	75.7	15.1	0.35	0.03
	100–200	12.7	12.5	0.35	0.003
52.5–42.5°S	0–100	42.6	6.0	0.37	0.004
	100–200	10.3	4.9	0.37	0.001
Total					0.68

<sup>a</sup>Water depth < 200 m.

**Table 3.** Annual CO Dark Production in Global Blue Waters<sup>a</sup>

Region	Layer (m)	Area (10 <sup>4</sup> km <sup>2</sup> )	T (°C)	Salinity	$a_{350}$ (m <sup>-1</sup> )	CO (Tg C a <sup>-1</sup> )
<i>Pacific Ocean</i>						
27.5–42.5°N	0–100	1507	14.77	34.0	0.096	0.15
12.5–27.5°N	0–50	2263	24.33	34.8	0.044	0.20
	50–150	2263	20.28	34.8	0.044	0.23
0–12.5°N	0–50	2921	27.02	34.4	0.068	0.59
	50–150	2921	20.26	34.7	0.068	0.45
12.5°S–0	0–50	2620	26.44	35.2	0.067	0.47
	50–200	2620	21.52	35.4	0.067	0.70
27.5–12.5°S	0–50	2299	23.24	35.6	0.046	0.18
	50–200	2299	20.23	35.6	0.046	0.35
32.5–27.5°S	0–100	694	18.30	35.2	0.065	0.08
Subtotal						3.39
<i>Atlantic Ocean</i>						
27.5–42.5°N	0–100	925	17.83	35.9	0.080	0.11
12.5–27.5°N	0–50	1215	24.62	36.5	0.055	0.13
	50–150	1215	21.35	36.7	0.052	0.16
0–12.5°N	0–50	976	26.22	35.5	0.087	0.22
	50–150	976	18.21	35.9	0.096	0.15
12.5°S–0	0–50	890	24.73	36.0	0.097	0.18
	50–150	890	17.85	35.8	0.074	0.10
27.5–12.5°S	0–50	937	22.12	36.3	0.061	0.08
	50–150	937	18.78	36.0	0.064	0.11
42.5–27.5°S	0–100	1056	14.88	35.1	0.091	0.10
Subtotal						1.34
<i>Indian Ocean</i>						
12.5–27.5°N	0–50	215	26.14	35.7	0.163	0.18
	50–600	212	17.38	35.9	0.163	0.28
0–12.5°N	0–50	840	27.73	34.8	0.088	0.24
	50–200	840	19.80	35.2	0.088	0.23
12.5°S–0	0–50	1300	27.16	34.6	0.061	0.24
	50–200	1300	19.03	35.0	0.061	0.22
12.5–27.5°S	0–50	1287	23.82	35.2	0.051	0.12
	50–150	1287	20.52	35.4	0.051	0.15
27.5–37.5°S	0–100	1038	16.93	35.5	0.079	0.11
Subtotal						1.76
Grand total						6.49

<sup>a</sup>Water depth > 200 m.

C a<sup>-1</sup>, or 0.46–1.50 Tg CO-C a<sup>-1</sup> by taking into account the  $\pm 32\%$   $a_{350}$ -associated uncertainty. This range corresponds to 5–15% of the speculative estimate of CO photoproduction from CDOM in global coastal waters ( $\sim 10$  Tg CO-C a<sup>-1</sup>) [Zafiriou *et al.*, 2003]. In a more recent study, C. Fichot and W. L. Miller (Quantifying marine photochemical fluxes using remote sensing: a global, monthly, depth-resolved climatology of carbon monoxide photoproduction, submitted to *Remote Sensing of Environment*, 2008) arrived at a global coastal CO photoproduction flux of  $\sim 2.9$  Tg CO-C a<sup>-1</sup>, in which case the dark source is equivalent to 16–52% of the photochemical source.

[25] An effort was made to evaluate the contribution of particles to abiotic, thermal CO production by poisoning whole water samples from station PAP. We tested three widely used poisons, potassium cyanide (KCN), mercury chloride (HgCl<sub>2</sub>), and sodium azide (NaN<sub>3</sub>), and found they all gave rise to artifacts. KCN and HgCl<sub>2</sub> inhibited CO production while NaN<sub>3</sub> promoted it. The inhibition or promotion aggravated nonlinearly with increasing concentrations of the poisons. The concentration ranges tested were, KCN: 2.0–30.0 mg L<sup>-1</sup>, HgCl<sub>2</sub> (saturated solution):

0.2–0.6 mL L<sup>-1</sup>, and NaN<sub>3</sub>: 0.2–0.5 g L<sup>-1</sup>. A comparison was made between poisoned (2.0 mg L<sup>-1</sup> KCN) whole water and poisoned (2.0 mg L<sup>-1</sup> KCN), 0.2- $\mu$ m-filtered water.  $Q_{co}$  in the filtered water was  $\sim 30\%$  lower than in the whole water. If poisoning affected CO productions by particles and dissolved materials equally, the CO dark production term could be substantially higher if particles-derived CO is included.

### 3.4. Implication for the Global Blue Water CO Budget

[26] Because the  $S$  (0.1–34.7) and  $a_{350}$  (0.23–15.32 m<sup>-1</sup>) ranges, on which equation (1) is based, are largely beyond the corresponding ranges of blue waters (depth > 200 m), extrapolation of equation (1) to the open ocean may lead to potentially large uncertainties. We caution the reader that the estimates made below for blue waters and global oceans are speculative and need verification and improvement in the future.

[27] The applicability of equation (1) to blue waters was validated to a limited extent with a sample from the Bermuda Atlantic Time series Study (BATS) site. The sample was collected at a depth of 40 m in late September 2007 and had an in situ  $T$ : 26.7°C,  $S$ : 36.43, pH: 8.22, and  $a_{350}$ : 0.072 m<sup>-1</sup>. It had been 0.2- $\mu$ m-filtered and stored cold for 69 days before being incubated (27°C) for  $Q_{co}$  determination. The production rate was measured to be 0.0025 nmol L<sup>-1</sup> h<sup>-1</sup> while predicted to be 0.0039 nmol L<sup>-1</sup> h<sup>-1</sup>. Note that the storage time of the BATS sample was 50 days longer than the average storage time (19 days) of the samples used to derive equation (1). This difference would reduce the predicted  $Q_{co}$  to 0.0034 nmol L<sup>-1</sup> h<sup>-1</sup> if the  $Q_{co}$ - $t$  relationship for the PAP sample (section 3.2.4) is applied. The measured value is hence 73% of the predicted value, a reasonably good match.

[28] To assess the CO dark production fluxes in blue waters on the basis of equation (1), the open oceans are divided into latitudinal zones and depth layers (Table 3) in the same manner as for coastal waters. Blue water pH is fixed at 8.1 and area-weighted annual mean  $T$  and  $S$  were obtained from *Levitus* [1982]. Open ocean surface  $a_{350}$  data were derived from the same remote-sensing algorithm as described in section 3.3. Subsurface  $a_{350}$  data for the North Atlantic are from *Nelson et al.* [2007] and for the South Atlantic from *Kitidis et al.* [2006]. Surface CDOM abundances in the Pacific and Indian Oceans are assumed to be the subsurface layers there, an assumption that is supported by limited available CDOM data from the equatorial Pacific [Simeon *et al.*, 2003] and by relatively larger data sets from the Atlantic [Nelson *et al.*, 1998, 2007].

[29] Zones and layers are omitted with  $Q_{co} \leq 8.0 \times 10^{-4}$  nmol L<sup>-1</sup> h<sup>-1</sup>, the upper limit predicted for the SLES samples with undetectable CO dark production (Table 1). This treatment leads to negligible CO dark production in high northern and southern latitudes and at depths > 200 m except in the subtropical Indian Ocean (Table 3). Among the three main blue water basins, the Pacific is the largest source (3.39 Tg CO-C a<sup>-1</sup>), due mainly to its large size, while the source strengths in the Atlantic (1.34 Tg CO-C a<sup>-1</sup>) and Indian Oceans (1.76 Tg CO-C a<sup>-1</sup>) are similar (Table 3). Vertically, production is slightly higher in the surface ML (3.37 Tg CO-C a<sup>-1</sup>) than below (3.12 Tg CO-C a<sup>-1</sup>). The global open ocean production is thus 6.49 Tg CO-C a<sup>-1</sup>.

Taking into account the sample storage effect, we estimated the blue water source to be in the range from 6.49 to 10.8 Tg CO-C a<sup>-1</sup>, or 4.41–14.3 Tg CO-C a<sup>-1</sup> by further including the  $a_{350}$ -linked uncertainty ( $\pm 32\%$ ).

[30] Summation of the coastal and blue water sources gives a global oceanic CO dark production of 4.87–15.8 Tg CO-C a<sup>-1</sup>, equivalent to 10–32% of the best available estimates of the global marine CO photoproduction flux ( $\sim 50$  Tg CO-C a<sup>-1</sup>) [Zafiriou *et al.*, 2003; Stubbins *et al.*, 2006a]. In the surface ML, where most photoproduction occurs and where CO is available for exchange with the atmosphere, the dark production term ranges from 2.66 to 8.62 Tg CO-C a<sup>-1</sup>, which are similar to or larger than the best available estimates (3.7–5.52 Tg CO-C a<sup>-1</sup>) of the global oceanic CO flux to the atmosphere [Bates *et al.*, 1995; Stubbins *et al.*, 2006b]. If dark and photo productions contribute to the CO flux proportionally according to their mixed layer source strengths, 5–17% of the CO flux would arise from dark production. Its upper limit equals the value (16.8%) of Kettle [2005] derived from modeling published CO profiles.

### 3.5. Steady State Deepwater [CO]

[31] In deep blue waters, dark production (2.12–6.88 Tg CO-C a<sup>-1</sup>) should essentially be balanced by microbial consumption, which generally follows first-order kinetics at low [CO] [Xie *et al.*, 2005]. Knowing the first-order uptake rate constant,  $k_{bio}$ , would allow to estimate the deep steady state [CO] (i.e.,  $Q_{co} \div k_{bio}$ ) or vice versa. Subsurface water (>100 m)  $k_{bio}$  data are rare. Jones [1991] determined  $k_{bio}$  from the surface to 900 m at a site in the Sargasso Sea. Unfortunately, the <sup>14</sup>C technique employed in that study could have substantially underestimated the obtained  $k_{bio}$  values [Xie *et al.*, 2005]. Using dark incubations of untreated whole samples collected in March at the BATS site, Kettle [1994] found no consistent depth dependence of  $k_{bio}$  and acquired a  $k_{bio}$  of 0.026 h<sup>-1</sup> at 200 m. This value is close to the rate constant (0.022 h<sup>-1</sup>) recently reported by Zafiriou *et al.* [2008] for the upper 200-m layer in the same area and season. The storage effect-corrected  $Q_{co}$  at 200 m at BATS was estimated as 0.0018 nmol L<sup>-1</sup> h<sup>-1</sup> using  $T = 19^\circ\text{C}$  [Zafiriou *et al.*, 2008] and  $a_{350} = 0.060 \text{ m}^{-1}$  (N. B. Nelson, unpublished data, 2000). The steady state [CO] is thus 0.07 nmol L<sup>-1</sup> on the basis of Kettle's  $k_{bio}$  value. This predicted [CO] is within the BATS' 200-m [CO] range in March (0.02–0.12 nmol L<sup>-1</sup>; mean:  $0.05 \pm 0.03$  nmol L<sup>-1</sup>) determined using improved CO sampling and analytical techniques [Zafiriou *et al.*, 2008]. In August 1999 at BATS, a  $k_{bio}$  of 0.028 h<sup>-1</sup> in the 100–200 m layer was inferred from a limited number of deep CO profiles (H. Xie *et al.*, unpublished data, 1999). Combining this  $k_{bio}$  value with  $Q_{co}$  computed from the concurrently measured 200-m  $T$  ( $\sim 19^\circ\text{C}$ ) and  $a_{350}$  (0.033 m<sup>-1</sup>) (N. B. Nelson, unpublished data, 1999) gives a steady state [CO] of 0.04 nmol L<sup>-1</sup>. This value agrees with the measured August 200-m CO concentrations (range: 0.011–0.053 nmol L<sup>-1</sup>; mean:  $0.03 \pm 0.01$  nmol L<sup>-1</sup>), which were comparable to the method's blank [Zafiriou *et al.*, 2008]. Hence, CO dark production, a potentially significant term in the global marine CO cycle, could be inadvertently ignored if judged only from its near blank level concentrations at depth. Note that the agreement between the predicted and measured steady state [CO]

indirectly supports the applicability of equation (1) to blue waters, but again to a limited extent because of the very limited number of cases available for such comparisons.

## 4. Summary and Conclusions

[32] This study represents the first systematic investigation of CO dark production in natural waters. CDOM was found to be a good proxy of CO precursors. Terrestrial organic substrates appeared to be more efficient than their marine counterparts with respect to CO dark production. The  $T$ -dependence of CO dark production obeyed the Arrhenius equation with the activation energy for freshwater being considerably higher than for seawater. The dark production rate remained relatively stable between pH 4–6 but increased steadily with further increasing pH, a phenomenon that is highly relevant to estuarine mixing. Contrary to CO photoproduction, ionic strength and iron exhibited little influence on the dark production. Using an empirical equation relating the dark production rate to  $a_{350}$ ,  $T$ ,  $S$ , and pH, we estimated the total CO dark production from DOM in the global coastal waters to be in the range 0.46–1.50 Tg CO-C a<sup>-1</sup>, equivalent to 16–52% of the global coastal water photochemical source. Extrapolation of the results to blue waters gives a speculative total oceanic (coastal plus blue water) CO dark production of 4.87–15.8 Tg CO-C a<sup>-1</sup>, which is significant to the best available estimate of global oceanic CO photoproduction of 50 Tg CO-C a<sup>-1</sup>. The dark source in the surface ML (2.66–8.62 Tg CO-C a<sup>-1</sup>) alone could account for the current best estimate of CO flux to the atmosphere. Available sub-ML microbial CO uptake data suggest that steady state [CO] at depth inferred from dark production are so low that they defy to be accurately quantified even by the best available sampling and analytical techniques.

[33] Potentially large uncertainties may exist in the current evaluation of global CO dark production since the empirical equation used to make the extrapolation was based on limited data obtained from an environment that is strongly influenced by terrestrial runoffs. Obviously, more blue water samples, in addition to the aforementioned BATS water, are needed to validate this equation. To improve the estimates, field measurements should be extended to other marine domains, particularly open oceans, to map CO dark production rates in diverse geographic regions; incubations should be carried out within the shortest time possible of sample collection to minimize sample storage effect; spatially and temporally denser subsurface CDOM measurements are required if this term remains essential in future extrapolations. Efforts should also be made to characterize processes responsible for the production of CO precursors. For closure studies of deepwater CO cycling, simultaneous measurements are required of CO dark production rates, consumption rate constants and profiles (with improved methods). Finally, the role of particles in the CO dark production budget needs to be further elucidated.

[34] **Acknowledgments.** S. Bélanger and R. Villeneuve assisted in CDOM absorbance measurement. G. Canuel analyzed salinity samples. O. Zafiriou, J. Dacey, and N. Levine assisted in the collection of the BATS sample. We thank the chief scientist, colleagues and the captain and crew of the *Coriolis II* cruise for their cooperation. We are also grateful to A. Stubbins and two anonymous reviewers for their insightful comments on



the manuscript. Y.Z. was supported by an ISMER graduate fellowship. This work was supported by H.X.'s grants from Natural Sciences and Engineering Research Council of Canada (NSERC) and the Canada Foundation for Innovation (CFI). This is a contribution to the research programs of the Institut des Sciences de la Mer de Rimouski (ISMER).

## References

- Babin, M., D. Stramski, G. M. Ferrari, H. Claustre, A. Bricaud, G. Obolensky, and N. Hoepffner (2003), Variations in the light absorption coefficients of phytoplankton, nonalgal particles, and dissolved organic matter in coastal waters around Europe, *J. Geophys. Res.*, *108*(C7), 3211, doi:10.1029/2001JC000882.
- Bates, T. S., K. C. Kelly, J. E. Johnson, and R. H. Gammon (1995), Regional and seasonal-variations in the flux of oceanic carbon monoxide to the atmosphere, *J. Geophys. Res.*, *100*, 23,093–23,101, doi:10.1029/95JD02737.
- Conrad, R., W. Seiler, G. Bunse, and H. Giehl (1982), Carbon monoxide in seawater (Atlantic Ocean), *J. Geophys. Res.*, *87*, 8839–8852, doi:10.1029/JC087iC11p08839.
- Doney, S. C., R. G. Najjar, and S. Stewart (1995), Photochemistry, mixing and diurnal cycles in the upper ocean, *J. Mar. Res.*, *53*, 341–369, doi:10.1357/0022240953213133.
- Fichot, C. (2004), Marine photochemistry from space, M.S. thesis, 237 pp., Dalhousie Univ., Halifax, Nova Scotia, Canada.
- Fichot, C. G., S. Sathyendranath, and W. L. Miller (2008), SeaUV and SeaUV<sub>C</sub>: Algorithms for the retrieval of UV/Visible diffuse attenuation coefficients from ocean color, *Remote Sens. Environ.*, *112*, 1584–1602.
- Flock, O. R., and M. O. Andreae (1996), Photochemical and non-photochemical formation and destruction of carbonyl sulfide and methyl mercaptan in ocean waters, *Mar. Chem.*, *54*, 11–26, doi:10.1016/0304-4203(96)00027-8.
- Gao, H. Z., and R. G. Zepp (1998), Factors influencing photoreactions of dissolved organic matter in a coastal river of the southeastern United States, *Environ. Sci. Technol.*, *32*, 2940–2946, doi:10.1021/es9803660.
- Hernes, P. J., and R. Benner (2003), Photochemical and microbial degradation of dissolved lignin phenols: Implications for the fate of terrigenous dissolved organic matter in marine environments, *J. Geophys. Res.*, *108*(C9), 3291, doi:10.1029/2002JC001421.
- Johnson, J. E., and T. S. Bates (1996), Sources and sinks of carbon monoxide in the mixed layer of the tropical South Pacific Ocean, *Global Biogeochem. Cycles*, *10*, 347–359, doi:10.1029/96GB00366.
- Jones, R. D. (1991), Carbon-monoxide and methane distribution and consumption in the photic zone of the Sargasso Sea, *Deep Sea Res., Part A*, *38*, 625–635, doi:10.1016/0198-0149(91)90002-W.
- Kettle, A. J. (1994), A model of the temporal and spatial distribution of carbon monoxide in the mixed layer, M.S. thesis, 146 pp., Mass. Inst. of Technol., Cambridge.
- Kettle, A. J. (2000), Comparison of dynamic models to predict the concentration of a photochemical tracer in the upper ocean as a function of depth and time, *Mar. Freshwater Res.*, *51*, 289–304, doi:10.1071/MF99146.
- Kettle, A. J. (2005), Diurnal cycling of carbon monoxide (CO) in the upper ocean near Bermuda, *Ocean Modell.*, *8*, 337–367, doi:10.1016/j.ocemod.2004.01.003.
- Kitidis, V., A. P. Stubbins, G. Uher, R. C. Upstill-Goddard, C. S. Law, and E. M. S. Woodward (2006), Variability of chromophoric organic matter in surface waters of the Atlantic Ocean, *Deep Sea Res., Part II*, *53*, 1666–1684.
- Levitus, S. (1982), *Climatological Atlas of the World Ocean*, NOAA, Silver Spring, Md.
- Lou, T. (2005), Photodegradation of dissolved organic matter and its influence on hydrophobic binding affinity, Ph.D. thesis, 127 pp., Ocean Univ. of China, Qingdao, China.
- Miller, W. L., and R. G. Zepp (1995), Photochemical production of dissolved inorganic carbon from terrestrial organic matter: Significance to the oceanic organic carbon cycle, *Geophys. Res. Lett.*, *22*, 417–420, doi:10.1029/94GL03344.
- Minor, E. C., J. Pothen, B. J. Dalzell, H. Abdulla, and K. Mopper (2006), Effects of salinity changes on the photodegradation and ultraviolet-visible absorbance of terrestrial dissolved organic matter, *Limnol. Oceanogr.*, *51*, 2181–2186.
- Mopper, K., and D. J. Kieber (2000), Marine photochemistry and its impact on carbon cycling, in *The Effects of UV Radiation in the Marine Environment*, edited by S. de Mora et al., pp. 101–129, Cambridge Univ. Press, New York.
- Mopper, K., J. Helms, A. Stubbins, N. Chen, E. Minor, and B. Dalzell (2006), Effect of pH and ionic strength on terrestrial DOM photoreactivity: Implications in estuarine DOM transformations, *Eos Trans. AGU*, *87*(36), Ocean Sci. Meet. Suppl., OS541–04.
- Moran, M. A., and R. G. Zepp (1997), Role of photoreactions in the formation of biologically labile compounds from dissolved organic matter, *Limnol. Oceanogr.*, *42*, 1307–1316.
- Nelson, N. B., D. A. Siegel, and A. F. Michaels (1998), Seasonal dynamics of colored dissolved materials in the Sargasso Sea, *Deep Sea Res., Part I*, *45*, 931–957, doi:10.1016/S0967-0637(97)00106-4.
- Nelson, N. B., D. A. Siegel, C. A. Carlson, C. Swan, W. M. Smethie, and S. Khatiwala (2007), Hydrography of chromophoric dissolved organic matter in the North Atlantic, *Deep Sea Res., Part I*, *54*, 710–731, doi:10.1016/j.dsr.2007.02.006.
- Nieke, B., R. Reuter, R. Heuermann, H. Wang, M. Babin, and J. C. Theriault (1997), Light absorption and fluorescence properties of chromophoric dissolved organic matter (CDOM), in the St. Lawrence Estuary (Case 2 waters), *Cont. Shelf Res.*, *17*, 235–252, doi:10.1016/S0278-4343(96)00034-9.
- Simeon, J., C. Roesler, W. S. Pegau, and C. Dupouy (2003), Sources of spatial variability in light absorbing components along an equatorial transect from 165°E to 150°W, *J. Geophys. Res.*, *108*(C10), 3333, doi:10.1029/2002JC001613.
- Stubbins, A., G. Uher, C. S. Law, K. Mopper, C. Robinson, and R. C. Upstill-Goddard (2006a), Open-ocean carbon monoxide photoproduction, *Deep Sea Res., Part II*, *53*, 1695–1705, doi:10.1016/j.dsr.2006.05.011.
- Stubbins, A., G. Uher, V. Kitidis, C. S. Law, R. C. Upstill-Goddard, and E. M. S. Woodward (2006b), The open-ocean source of atmospheric carbon monoxide, *Deep Sea Res., Part II*, *53*, 1685–1694, doi:10.1016/j.dsr.2.2006.05.010.
- Tremblay, L. (2003), Geochemical and analytical contributions in the study of humic substances from the St. Lawrence marine system, Ph.D. thesis, 351 pp., Université du Québec à Rimouski, Rimouski, Canada.
- Von Hobe, M., G. A. Cutter, A. J. Kettle, and M. O. Andreae (2001), Dark production: A significant source of oceanic COS, *J. Geophys. Res.*, *106*, 31,217–31,226, doi:10.1029/2000JC000567.
- Xie, H., S. S. Andrews, W. R. Martin, J. Miller, L. Ziolkowski, C. D. Taylor, and O. C. Zafiriou (2002), Validated methods for sampling and headspace analysis of carbon monoxide in seawater, *Mar. Chem.*, *77*, 93–108, doi:10.1016/S0304-4203(01)00065-2.
- Xie, H., O. C. Zafiriou, W. J. Cai, R. G. Zepp, and Y. C. Wang (2004), Photooxidation and its effects on the carboxyl content of dissolved organic matter in two coastal rivers in the southeastern United States, *Environ. Sci. Technol.*, *38*, 4113–4119, doi:10.1021/es035407t.
- Xie, H., O. C. Zafiriou, T. P. Umile, and D. J. Kieber (2005), Biological consumption of carbon monoxide in Delaware Bay, NW Atlantic and Beaufort Sea, *Mar. Ecol. Prog. Ser.*, *290*, 1–14, doi:10.3354/meps290001.
- Xie, H., S. Bélanger, S. Demers, W. F. Vincent, and T. N. Papakyriakou (2008), Photobiogeochemical cycling of carbon monoxide in the southeastern Beaufort Sea in spring and autumn, *Limnol. Oceanogr.*, in press.
- Zafiriou, O. C., S. S. Andrews, and W. Wang (2003), Concordant estimates of oceanic carbon monoxide source and sink processes in the Pacific yield a balanced global “blue-water” CO budget, *Global Biogeochem. Cycles*, *17*(1), 1015, doi:10.1029/2001GB001638.
- Zafiriou, O. C., H. Xie, N. B. Nelson, R. G. Najjar, and W. Wang (2008), Diel carbon monoxide cycling in the upper Sargasso Sea near Bermuda at the onset of spring and in midsummer, *Limnol. Oceanogr.*, *53*, 835–850.
- Zhang, Y., H. Xie, and G. Chen (2006), Factors affecting the efficiency of carbon monoxide photoproduction in the St. Lawrence estuarine system (Canada), *Environ. Sci. Technol.*, *40*, 7771–7777, doi:10.1021/es0615268.

G. Chen, College of Chemistry and Chemical Engineering, Ocean University of China, Qingdao 266100, China.

C. G. Fichot, Department of Marine Sciences, University of Georgia, Athens, GA 30602, USA.

H. Xie and Y. Zhang, Institut des Sciences de la Mer de Rimouski, Université du Québec à Rimouski, Rimouski, QC G5L 3A1, Canada. (huixiang\_xie@uqar.qc.ca)